This is a repository copy of *Modelling and analysis of inter-turn short-circuit fault of PM machines with parallel-connected coils*.

White Rose Research Online URL for this paper:
https://eprints.whiterose.ac.uk/194842/

Version: Accepted Version

Article:
Mei, Z., Li, G.-J. orcid.org/0000-0002-5956-4033, Zhu, Z.Q. et al. (3 more authors) (2023) Modelling and analysis of inter-turn short-circuit fault of PM machines with parallel-connected coils. IEEE Transactions on Energy Conversion. ISSN 0885-8969

https://doi.org/10.1109/TEC.2023.3234332

© 2023 IEEE. Personal use of this material is permitted. Permission from IEEE must be obtained for all other users, including reprinting/ republishing this material for advertising or promotional purposes, creating new collective works for resale or redistribution to servers or lists, or reuse of any copyrighted components of this work in other works. Reproduced in accordance with the publisher's self-archiving policy.

Reuse
Items deposited in White Rose Research Online are protected by copyright, with all rights reserved unless indicated otherwise. They may be downloaded and/or printed for private study, or other acts as permitted by national copyright laws. The publisher or other rights holders may allow further reproduction and re-use of the full text version. This is indicated by the licence information on the White Rose Research Online record for the item.

Takedown
If you consider content in White Rose Research Online to be in breach of UK law, please notify us by emailing eprints@whiterose.ac.uk including the URL of the record and the reason for the withdrawal request.

eprints@whiterose.ac.uk
https://eprints.whiterose.ac.uk/

Modelling and Analysis of Inter-Turn Short-Circuit Fault of PM Machines with Parallel-Connected Coils

Z. T. Mei[1], G. J. Li[1], *Senior Member*, *IEEE*, Z. Q. Zhu[1], *Fellow*, *IEEE*, R. Clark[2], A. Thomas[2] and Z. Azar[2]
[1]Department of Electronic and Electrical Engineering, The University of Sheffield, Sheffield, UK
[2]Siemens Gamesa Renewable Energy Limited, Sheffield, UK
g.li@sheffield.ac.uk

***Abstract*—This paper presents a general analytical fault model in a compact matrix form for surface-mounted permanent magnet (SPM) machines with parallel-connected coils, which is useful to study the machine performance under the inter-turn short circuit (ITSC) fault. To simplify the fault model, the multiphase Clarke transformation has been proposed. In the model, the branch currents rather than the phase currents are employed as state variables to describe machine behaviours under fault. Additionally, self- and mutual-inductances are obtained by winding function approach (WFA) plus slot permeance method. The proposed analytical fault model is applied to a 3 kW 96-slot 32-pole SPM machine and validated by time-stepping FE simulations. A small scale 12-slot 4-pole SPM machine prototype has also been built to further validate the accuracy of the proposed fault model.**

***Index Terms*—branch currents, inter-turn short-circuit, multiphase Clarke transformation, surface-mounted permanent magnet machines.**

I. Introduction

As the cumulative installed wind power capacity in the global market is increasing rapidly, reducing the cost of energy becomes more and more important. It has been reported that the operation and maintenance costs have a relatively large share of the total income of a wind farm (10% to 25%) [1], [2]. If the wind power generator, one of the major components of a wind turbine system, has a failure and cannot be detected timely, it may escalate to more serious system level fault and incur more costly and difficult maintenance work. Therefore, it is necessary to investigate various faults of large wind power generators. One early literature review [3] has shown that apart from the bearing fault, winding fault is most prevalent one in wind power generators. In fact, there are five major types of winding fault for wind power generators and the inter-turn short-circuit (ITSC) fault was deemed to be the incipient stage of other severer faults [4]. Furthermore, it is often difficult to detect, identify, and localize the ITSC fault. The short-circuit current caused by it could be many times higher than the rated current, leading to serious local overheating, and potential magnet irreversible demagnetization. If the ITSC fault could be detected and mitigated before it worsens, the generators could be protected to reduce the amount of maintenance work and cost. Hence, it is meaningful to study the ITSC fault. To this end, the physics-based fault modelling has attracted increasing interest from both academia and industry. This is mainly because it can provide a powerful insight into the fault phenomena.

In [5], the characteristics of three major methods such as (1) winding function approach (WFA), (2) finite element analysis (FEA), and (3) magnetic equivalent circuit (MEC) [6]–[8] to model the machine behavior under ITSC fault were described. In [5], a general analytical model of surface-mounted permanent magnet (SPM) machines with series-connected coils under ITSC fault was proposed, in which the inductances neglecting end-turn leakage component under fault were calculated by analytical method, i.e., WFA plus slot permeance method. However, the fault modelling of medium and large-power electrical machines equipped with series-parallel-connected windings, although much more complicated, is more desirable [9]–[11]. In [9], the transient behaviour of salient-pole synchronous machines with internal stator winding faults including ITSC fault was modelled by the multi-loop circuit method. In the developed fault model, stator branch currents were transformed into loop currents and used as state variables. The authors in [9] also concluded without proof that the accuracy of the simulation results using inductances determined by analytical techniques was similar to those with inductances obtained by linear FEA. In [10], the authors calculated the machine inductances of a synchronous machine with series-parallel windings based on the WFA to study different internal faults like ground fault and phase-to-phase short circuit fault. In [11], the author explained the reason for choosing branch currents as state variables when a machine was subject to one type of internal faults. Furthermore, eight types of faults including the ITSC fault for a 370MVA salient-pole synchronous generator with fractional-slot winding are simulated using a Hypersim real-time simulator. However, the inductance calculation involved and the large number of first-order differential equations required to establish the fault model make the internal fault modelling of large salient-pole synchronous generators quite complex and challenging. Furthermore, not much physical insight is provided. Other researchers in [12] tried to simplify the calculation of large number of inductances in the analytical fault model. However, their assumptions may not be easily applicable to other types of machines. Despite the progress made by the authors in [9]–[12], no general fault model has been developed, which is mainly due to the saliency and complex winding arrangement of synchronous machines. In [13], the authors proposed ITSC fault models of fractional-slot SPM machines employing series and parallel winding connections. It was assumed that all branch currents in healthy phases (phases B and C) were equal when the ITSC fault occurred in one of the faulty phase (phase A) branches of a 6-pole-9-slot SPM motor. This may not be true for integer-slot SPM machines. In [14], the authors analysed

different modes of ITSC fault in SPM motors with multi-strand windings and made the same assumption as that of [13]. However, both [13] and [14] did not provide a relatively simple analytical method to obtain the inductances in the fault model.

Unlike the progress made by [9]–[11], [13], [14], this paper proposes a general analytical model in a compact matrix form for SPM machines with parallel-connected coils under inter-turn short circuit (ITSC) fault. To simplify the fault model, the multiphase Clarke transformation has been proposed. It is worth mentioning that, in this paper, core saturation has been neglected for inductance calculation using the developed analytical technique and for fault model simplification using the multiphase Clarke transformation. In the fault model, branch currents rather than the phase currents are used as state variables to describe machine behaviour under ITSC fault. In addition, to simplify the process of inductance calculation, the winding of analysed SPM machines is integer slot, single-layer, and distributed (slot/pole/phase (SPP) equal to 1), which is often the case for winding structures adopted by large PM wind power generators. Based on this simple winding configuration, inductances of the fault model are obtained by winding function approach (WFA) plus slot permeance method. Particular attention has also been paid to the one-coil short-circuit fault, which is equivalent to the phase short-circuit fault for the winding configuration (one coil per parallel branch) investigated in this paper. The proposed fault machine model is applied to a 3 kW 96-slot 32-pole SPM machine, which is built in Matlab/Simulink and validated by time stepping FE simulations. A small scale 12-slot 4-pole SPM machine has also been built to validate the proposed model.

II. MODELLING OF ITSC FAULT OF SPM WIND GENERATOR

A. Analytical Modelling

One example of parallel-connected coils of the studied PM machine under ITSC fault is shown in Fig. 1, where the fault is assumed to occur in the first branch of phase A. As mentioned previously, the winding of the analyzed SPM machines is integer slot, single-layer, and distributed, as shown in Fig. 2. meaning that the number of coils in one phase winding is identical to the number of pole pairs, p (for the studied 96-slot 32-pole SPM machine, $p = 16$). This can be seen in Fig. 1, i.e., when one parallel branch has one coil only, 16 parallel branches will contain 16 coils in total.

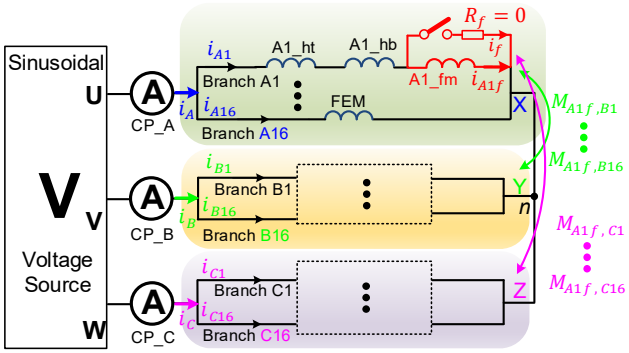

Fig. 1 Circuit schematic of the studied PM machines under ITSC fault.

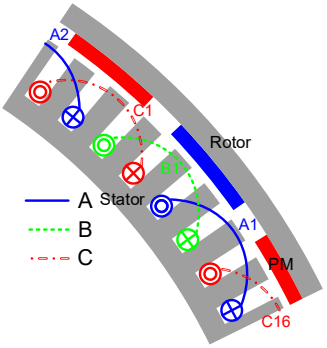

Fig. 2 Cross-section of the studied SPM machine with overlapping winding.

In addition, to simplify the analyses, the short-circuited turns of the faulty coil A1 are labeled as A1_fm, and the remaining healthy turns are marked as A1_ht and A1_hb, the meanings of which will be detailed in section II.B. The mutual inductances between the short-circuited turns and other coils such as $M_{A1f,A16}$, $M_{A1f,B1}$, and $M_{A1f,C16}$, etc. are also shown in Fig. 1.

From Fig. 1, the circuit branch voltage equations representing the relationship between branch-to-neutral voltages, EMFs, and branch currents under ITSC fault can be written in a compact matrix form as

$$\begin{bmatrix}\mathbf{v}_A\\ \mathbf{v}_B\\ \mathbf{v}_C\end{bmatrix} = \begin{bmatrix}\mathbf{L}_{AA} & \mathbf{M}_{AB} & \mathbf{M}_{AC}\\ \mathbf{M}_{BA} & \mathbf{L}_{BB} & \mathbf{M}_{BC}\\ \mathbf{M}_{CA} & \mathbf{M}_{CB} & \mathbf{L}_{CC}\end{bmatrix}\frac{\mathrm{d}}{\mathrm{d}t}\begin{bmatrix}\mathbf{i}_A\\ \mathbf{i}_B\\ \mathbf{i}_C\end{bmatrix} + R_{\mathrm{coil}}\begin{bmatrix}\mathbf{i}_A\\ \mathbf{i}_B\\ \mathbf{i}_C\end{bmatrix} + \begin{bmatrix}\mathbf{e}_A\\ \mathbf{e}_B\\ \mathbf{e}_C\end{bmatrix} - \begin{bmatrix}R_{A1f}\\ 0\\ \vdots\\ 0\end{bmatrix} i_f - \begin{bmatrix}\boldsymbol{M}_{Af}\\ \boldsymbol{M}_{Bf}\\ \boldsymbol{M}_{Cf}\end{bmatrix}\frac{\mathrm{d}i_f}{\mathrm{d}t} \tag{1}$$

where **v, i,** and **e** are column vectors representing branch-to-neutral voltages (v), branch back-EMFs (e) or branch currents (i) for the phases A, B and C windings. Each column vector has p entries, and p is the number of pole pairs as mentioned previously. For example, the column vector $\mathbf{v}_A = [v_{A1} \quad v_{A2} \quad \cdots \quad v_{Ap}]^T$ has a size of $p \times 1$. Additionally, i_f is the current in the short-circuit path as shown in Fig. 1. As for $\mathbf{L}_{AA}$, $\mathbf{M}_{AB}$, $\mathbf{M}_{AC}$ and $\mathbf{M}_{BC}$, they describe the inductive coupling between two coils/branches in the same phase or in two different phases. In this paper, they are termed as branch inductance matrices (see appendix A). In addition, R_{coil} in (1) is the coil resistance, and R_f is the contact resistance between short-circuited points. In the following case studies for the 3 kW machine, R_f is set to be zero for simplicity.

For the short-circuited path, the voltage equation is expressed as

$$\begin{aligned}&(R_f + R_{A1f})i_f + L_{A1f,A1f}\frac{\mathrm{d}i_f}{\mathrm{d}t} - e_{A1f} - R_{A1f}i_{A1}\\ &= (\boldsymbol{M}_{Af})^T\frac{\mathrm{d}\mathbf{i}_A}{\mathrm{d}t} + (\boldsymbol{M}_{Bf})^T\frac{\mathrm{d}\mathbf{i}_B}{\mathrm{d}t} + (\boldsymbol{M}_{cf})^T\frac{\mathrm{d}\mathbf{i}_C}{\mathrm{d}t}\end{aligned} \tag{2}$$

Regarding the short-circuited turns, R_{A1f}, $L_{A1f,A1f}$, and e_{A1f} are their resistance, self-inductance, and back EMF. It could be easily found that $e_{A1f} = \mu_1 e_A$, in which the coil faulty turn ratio in one phase winding is defined as $\mu_1 = n_f/n_c$ for the studied integer-slot SPM machines. As for n_f and n_c, they are the number of short-circuited turns in one coil and the total number of turns per coil, respectively. The last remaining terms,

$\boldsymbol{M}_{Af}$, $\boldsymbol{M}_{Bf}$, and $\boldsymbol{M}_{Cf}$, are faulty inductance vectors related to the short-circuited turns (see appendix A).

For the wye-connected stator windings with parallel coil connection, the sum of three phase currents must be zero as described by

$$\sum_{k=1}^{p} i_{Ak} + \sum_{k=1}^{p} i_{Bk} + \sum_{k=1}^{p} i_{Ck} = 0 \tag{3}$$

Furthermore, if the branch back EMFs in (1) contain harmonics and no neutral line is introduced, then the branch-to-neutral voltages cannot be directly obtained from the line voltages under ITSC fault. Considering the "circulant" characteristic of branch inductance matrices (see appendix A) and current constraints, the sum of the 3 phase voltages will be

$$\begin{aligned} &v_A + v_B + v_C = (e_A + e_B + e_C) \\ &-\frac{1}{p}\left[R_{A1f} i_f + \left(\sum_{k=1}^{p} \left(\mathbf{M}_{Af} + \mathbf{M}_{Bf} + \mathbf{M}_{Cf}\right)_k\right) \frac{\mathrm{d}i_f}{\mathrm{d}t}\right] \end{aligned} \tag{4}$$

where v_A, v_B, and v_C are three branch-to-neutral voltages. On the other hand, e_A, e_B, and e_C are the three branch back-EMFs. It is worth noting that all the branch-to-neutral voltages belonging to the same phase such as v_{A1} to v_{Ap} and the corresponding branch back-EMFs are equal in the study. In the meantime, to be concise, $\left(\mathbf{M}_{Af} + \mathbf{M}_{Bf} + \mathbf{M}_{Cf}\right)_k$ is used to denote the k^{th} element of the sum of three faulty inductance vectors $\boldsymbol{M}_{Af}$, $\boldsymbol{M}_{Bf}$, and $\boldsymbol{M}_{Cf}$.

In addition, line voltages v_{AB} and v_{BC} can be expressed in terms of branch-to-neutral voltages v_A and v_B as

$$v_{AB} = v_A - v_B \tag{5}$$

$$v_{BC} = v_B - v_C = v_A + 2v_B - (v_A + v_B + v_C) \tag{6}$$

Equations (4), (5), and (6) can be used to find the phase voltages (or branch-to-neutral voltages) from line voltages.

Once the currents in the healthy and faulty windings are determined, the torque under ITSC fault can be calculated by

$$T_e = p\frac{(\mathbf{e}_A)^T \mathbf{i}_A + (\mathbf{e}_B)^T \mathbf{i}_B + (\mathbf{e}_C)^T \mathbf{i}_C - e_{A1f} i_f}{\omega_r} + T_{cog} \tag{7}$$

where ω_r is the rotor electrical speed (rad/s), T_{cog} is the cogging torque calculated by using FEA.

From the above equations for the fault model, it can be seen that the complexity of the analytical fault model using branch currents in stationary reference frame depends on the number of parallel branches. It is worth noting that the number of differential equations in the equivalent first-order system to describe the machine behavior under ITSC fault is $3p + 2$ for the studied machine with parallel-connected coils. The larger the number of parallel branches, the more effort is required to build the analytical fault model in Matlab/Simulink. In section 0, one model simplification method using the multiphase Clarke transformation will be proposed to significantly reduce the model complexity.

B. FE Modelling

To verify the results obtained by the proposed analytical fault model, 2D FE simulations (using JMAG software package) for the outer rotor 3 kW 96-slot 32-pole SPM machine with parallel coils have been carried out in this paper. Considering the asymmetric three phase windings of the machine under ITSC fault, full rather than partial FE model is employed and illustrated in Fig. 3, in which only part of the full model is used to show the potential location of the ITSC fault more clearly.

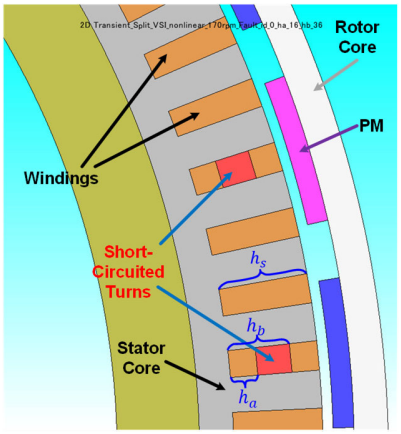

Fig. 3 Cross-sectional view of the 3 kW machine under the ITSC fault for FE simulations.

Additionally, the faulty machine is fed by voltage sources (as shown in Fig. 1) to more accurately predict the changes in phase currents and short-circuit current in FE simulations. The coil having ITSC fault shown in Fig. 3 is represented by three FEM coils, as illustrated in Fig. 1. One of the three FEM coils represents the remaining healthy turns at the bottom of the two slots where ITSC fault occurs, marked as A1_hb, and one at the top, named as A1_ht. Furthermore, the short-circuited turns in the middle are described by the A1_fm FEM coil. This arrangement will lead to balanced three phase back EMFs when the switch in Fig. 1 is open, i.e., the machine is healthy.

III. Inductance Calculation

One of the most important tasks of fault modeling is to determine the model parameters, especially the inductances in all branch inductance matrices. Experimental measurement and theoretical calculation are two typical ways to obtain inductances in the machine model.

In the past, for the purpose of machine control, the equivalent phase self- and mutual inductances or *dq*-axis inductances of healthy machines were often measured, which represent the combined effect of all elements in branch inductance matrices. However, under fault, it is required that the value of every individual element of branch inductance matrices is known prior to establishing the fault model. When large number of fault scenarios need to be investigated, the measurement of individual inductance element in the branch inductance matrices will become impractical. In addition, it is not realistic to measure many inductances at machine design stage. Due to these reasons, theoretical calculation especially analytical calculation of inductances without considering core saturation in those branch inductance matrices as a first approximation becomes important for initial study of ITSC fault modelling.

A. Calculation of Inductances

In [15], the three components of phase self- and mutual inductances are:

$$\begin{cases} L_{ph} = L_g + L_{ls} = L_g + L_{slot} + L_{end} \\ M_{ph} = M_g + M_{ls} = M_g + M_{slot} + M_{end} \end{cases} \quad (8)$$

where L_g and M_g are the air-gap components, L_{ls} and M_{ls} are the leakage components, respectively. L_{slot} and M_{slot} are the slot-leakage components, and L_{end} and M_{end} are the end-turn leakage components, respectively. It is worth mentioning that, in this paper, for the 3kW machine, the end-turn leakage component has been neglected due to relatively shorter end-windings. However, in the experimental validation of section VI, a detailed 3D FE modelling has been carried out for a small-scale prototype machine with much longer end-windings in relation to its active windings.

The air-gap component of inductances can be calculated by WFA [16]:

$$L_{ij} = \frac{\mu_0 r_e l_e}{g_e} \int_0^{2\pi} N_i(\phi_s) N_j(\phi_s)\, d\phi_s \quad (9)$$

where l_e is the effective stator stack length, r_e is the mean air-gap radius, g_e is the effective air-gap length, μ_0 is the permeability of free space. The calculation of r_e and g_e can be found in [15]. $N_i(\phi_s)$ and $N_j(\phi_s)$ are the winding functions of the i^{th} and j^{th} windings, respectively. When an ITSC fault happens, the healthy coil A1 is divided into two parts: faulty turns and remaining healthy turns. The corresponding winding functions after fault is illustrated in Fig. 4, which will be used to calculate the air-gap component of inductances in these two "coils" with different numbers of turns.

After determining the winding functions of other coils according to the winding layout shown in Fig. 2, all elements of the branch inductance matrices can be evaluated by calculating the air-gap and slot-leakage inductances separately, using similar method as in [5]. It is worth noting that these branch inductance matrices are all circulant matrices (see appendix A), meaning that once the elements in the first row of a circulant matrix are known, all the elements of the whole matrix can be determined. The final results are given as

$$\begin{cases} L_{A1A1} = L_{B1B1} = L_{C1C1} = L_1 \ (j = 1, 2, \cdots, p) \\ M_{A1Aj} = M_{B1Bj} = M_{C1Cj} = M_1 \ (j = 2, 3, \cdots, p) \\ M_{A1B1} = M_{B1C1} = M_{A1Cp} = M_2 \\ M_{A1Bj} = M_{B1Cj} = M_1 \ (j = 2, 3, \cdots, p) \\ M_{A1Cj} = M_{A1C1} = M_1 \ (j = 2, 3, \cdots, p-1) \end{cases} \quad (10)$$

with

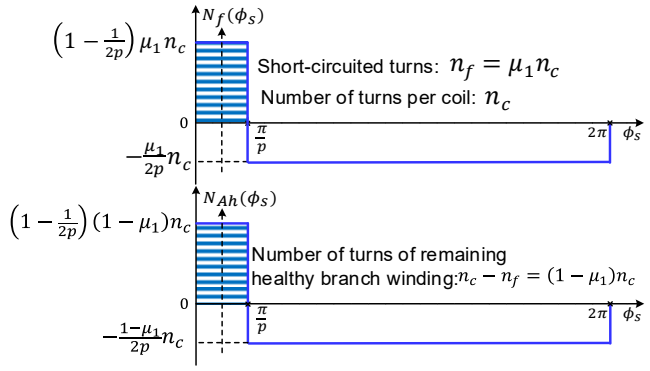

Fig. 4 Winding functions of faulty coil/branch A1 in Phase A.

$$\begin{cases} L_1 = \frac{\mu_0 r_e l_e}{g_e} \frac{(2p-1)}{2p^2} \pi (n_c)^2 + 2(n_c)^2 \mu_0 l_e \left[\frac{h_s}{3S_\omega}\right] \\ M_1 = \frac{\mu_0 r_e l_e}{g_e} \left(-\frac{1}{2p^2}\right) \pi (n_c)^2 \\ M_2 = \frac{\mu_0 r_e l_e}{g_e} \left(\frac{2p-3}{6p^2}\right) \pi (n_c)^2 \end{cases} \quad (11)$$

As for the elements in the faulty inductance vectors, they are redefined as

$$\begin{cases} L_{A1f,A1f} + M_{A1h,A1f} = L_{11} \\ M_{B1,A1f} = M_{Cp,A1f} = M_{22} \\ M_{Aj,A1f} = M_{Bj,A1f} = M_{11} \ (j = 2, 3, \cdots, p) \\ M_{Cj,A1f} = M_{11} \ (j = 1, 2, \cdots, p-1) \end{cases} \quad (12)$$

where the definition of these faulty inductances related to the short-circuited turns ($A1f$) can be found in appendix A. In terms of calculating $L_{A1f,A1f}$ and $M_{A1h,A1f}$, the air-gap and slot-leakage inductance components (indicated by subscripts "g" and "slot", respectively) same as those shown in [5] have to be calculated separately as follows

$$L_{11} = L_{A1f,A1f} + M_{A1h,A1f} = \left(L_{A1f,A1f}\right)_g + \left(L_{A1f,A1f}\right)_{slot} + \left(M_{A1h,A1f}\right)_g + \left(M_{A1h,A1f}\right)_{slot} \quad (13)$$

with

$$\left(L_{A1f,A1f}\right)_g = \frac{\mu_0 r_e l_e}{g_e} \frac{(2p-1)}{2p^2} (\mu_1)^2 \pi (n_c)^2 \quad (14)$$

$$\left(L_{A1f,A1f}\right)_{slot} = 2\mu_0 l_e \left(\frac{n_c}{h_s}\right)^2 \frac{(h_b - h_a)^2}{S_\omega} \left(h_s - \frac{1}{3}h_a - \frac{2}{3}h_b\right) \quad (15)$$

$$\left(M_{A1h,A1f}\right)_g = \frac{\mu_0 r_e l_e}{g_e} \frac{(2p-1)}{2p^2} [\mu_1 - (\mu_1)^2] \pi (n_c)^2 \quad (16)$$

$$\left(M_{A1h,A1f}\right)_{slot} = 2\mu_0 l_e \left(\frac{n_c}{h_s}\right)^2 \left[\frac{h_a(h_b - h_a)^2}{2S_\omega} + \frac{(h_b - h_a)}{2S_\omega} \{(h_s - h_b + h_a)^2 - h_a^2\}\right] \quad (17)$$

In (13) to (17), h_s is the slot height, h_a and h_b represent the fault locations along the slot, as shown in Fig. 3, and $n_f = n_c(h_b - h_a)/h_s$ represents the number of short-circuited turns.

In addition, M_{22} and M_{11} in (12) can be expressed as

$$\begin{cases} M_{22} = \frac{\mu_0 r_e l_e}{g_e} \frac{(2p-3)}{6p^2} \mu_1 \pi (n_c)^2 \\ M_{11} = -\frac{\mu_0 r_e l_e}{g_e} \frac{\mu_1}{2p^2} \pi (n_c)^2 \end{cases} \quad (18)$$

Equation (18) clearly shows that the mutual inductances between the short-circuited turns and other healthy coils do not have slot-leakage inductance component. With the above equations, all the inductance elements in the fault model have now been determined.

B. Results of Inductance Calculation

The machine specifications are given in Table I. The winding configuration of the 3 kW SPM machine has been changed from series-connected coils in [5] to parallel-connected coils. In addition, the inductance characteristics of the 3 kW 96-slot 32-pole SPM healthy machine with parallel-connected coils calculated by FE simulations and analytical approach are shown in Fig. 5. To be consistent with the analytical method in determining the inductances, in the FE model, all permanent magnets have been replaced by air, and the stator and rotor core

Table I Specifications of the studied SPM machine

Rated power(kW)	3	Numbers of slots/poles	96/32
Rated speed (rpm)	170	Rotor outer diameter (mm)	426.4
Line voltage (Vrms)	43.1	Stator outer diameter (mm)	401.1
Phase current (Arms)	40	Airgap length (mm)	2
Series turns/coil	52	Stack length (mm)	110

are assumed to be linear magnetic material with a relative permeability $\mu_r = 10000$. Only the coil A1 is excited by 1A DC current.

It should be mentioned that $\boldsymbol{L}_{AA} = \boldsymbol{L}_{BB} = \boldsymbol{L}_{CC}$ and $\boldsymbol{M}_{AB} = \boldsymbol{M}_{BC}$ due to symmetrical overlapping windings adopted by the studied SPM machine. Considering the large number of elements in a branch inductance matrix and the circulant property of these branch inductance matrices, only the absolute values [see Fig. 5 (a)] and the relative errors [see Fig. 5(b)] of inductances related to A1 coil are shown in Fig. 5. The relative error $[(M_{AjA1})_{\mathrm{RE}}]$ using M_{AjA1} as an example in Fig. 5(b) is given by

$$(M_{AjA1})_{\mathrm{RE}} = \frac{(M_{AjA1})_{\mathrm{Analytical}} - (M_{AjA1})_{\mathrm{FE}}}{(M_{AjA1})_{\mathrm{FE}}} \times 100 \qquad (19)$$

where $(M_{AjA1})_{\mathrm{Analytical}}$ is the mutual inductance calculated by analytical approach, and $(M_{AjA1})_{\mathrm{FE}}$ is obtained by FE simulations.

From Fig. 5(b), the following conclusions could be drawn:

- The self-inductance can be accurately predicted with a relative error of around 5%.
- The relative errors of mutual inductances between two adjacent coils are generally the smallest, which is smaller than 20%.
- The relative errors of mutual inductances between two coils farthest apart from each other is the biggest, up to 50%.

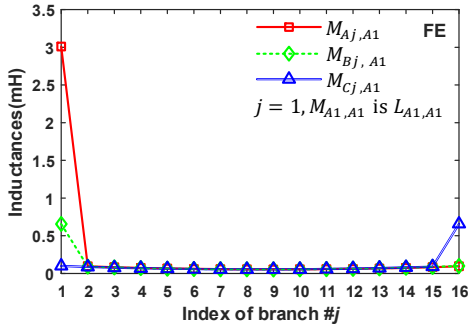

(a)

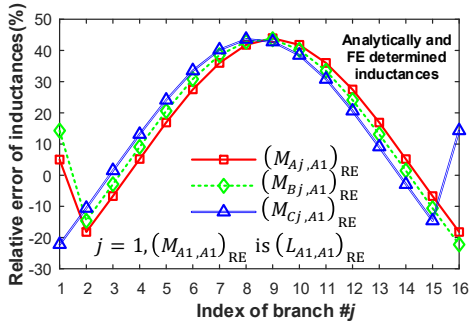

(b)

Fig. 5 Characteristics of inductances between A1 branch/coils and other branches/coils. (a) Absolute values and (b) relative errors.

Table II Equivalent self- and mutual-inductances (mH) of 3-phase windings

Method	L_{AA}	M_{AB}	M_{AC}
FE	0.1233	-0.02388	-0.02386
Analytical	0.1246	-0.02589	-0.02589
Relative error (%)	1.1	8.4	8.4

However, when two coils/branches are farther apart (the difference between the indices of branches will be bigger), their mutual inductances are much smaller compared to coils close to each other, as shown in Fig. 5(a). Therefore, although larger relative error is observed between some analytically calculated and FE inductances, this may not have a significant impact on the performance prediction such as healthy and short-circuit currents, torque, etc.

A further calculation of the equivalent phase self- and mutual inductances of 3-phase windings has been carried out, and it is shown in Table II. The calculation of the equivalent inductances of 3-phase windings with parallel-connected coils will be detailed in the section IV.A. Again, as explained previously, the much smaller differences in equivalent phase self- and mutual-inductances of 3-phase windings indicate that there would only be small errors in predicting phase currents of healthy machines by analytical and linear FE models. On the other hand, the results of relative errors of inductances between short-circuited turns and other coils are very much the same as those shown in Fig. 5, i.e., similar conclusions can also be made. It should be mentioned that all the inductance results are obtained without considering core saturation.

IV. Model Simplification Using Multiphase Clarke Transformation

Although the fault model in a compact matrix form is proposed using branch currents as state variables in the stationary reference frame, not much physical insight can be provided. In addition, it is difficult to build the fault model using Matlab/Simulink if the number of pole pairs is large. Therefore, it would be much better if the fault model could be simplified. After all the branch inductance matrices are determined analytically, it is found that all of them are circulant matrices like those of a healthy multiphase machine. Therefore, when original branch currents, voltages, and back-EMFs are transformed into new variables using multiphase Clarke transformation matrix $\boldsymbol{C}$ (see appendix B), the fault model may be simplified. This simplification process can be expressed as

$$\begin{bmatrix} \mathbf{f}'_A \\ \mathbf{f}'_B \\ \mathbf{f}'_C \end{bmatrix} = \begin{bmatrix} \boldsymbol{C} & \mathbf{0} & \mathbf{0} \\ \mathbf{0} & \boldsymbol{C} & \mathbf{0} \\ \mathbf{0} & \mathbf{0} & \boldsymbol{C} \end{bmatrix} \begin{bmatrix} \mathbf{f}_A \\ \mathbf{f}_B \\ \mathbf{f}_C \end{bmatrix} \qquad (20)$$

where $\mathbf{f}'_A$, $\mathbf{f}'_B$, $\mathbf{f}'_C$ are the corresponding transformed branch current, voltage, and back-EMF vectors. In this paper, the multiphase Clarke transformation matrix $\boldsymbol{C}$ adopts the power invariant form, meaning $\boldsymbol{C}^{-1} = \boldsymbol{C}^T$, so that

$$\begin{bmatrix} \mathbf{f}_A \\ \mathbf{f}_B \\ \mathbf{f}_C \end{bmatrix} = \begin{bmatrix} \boldsymbol{C}^T & \mathbf{0} & \mathbf{0} \\ \mathbf{0} & \boldsymbol{C}^T & \mathbf{0} \\ \mathbf{0} & \mathbf{0} & \boldsymbol{C}^T \end{bmatrix} \begin{bmatrix} \mathbf{f}'_A \\ \mathbf{f}'_B \\ \mathbf{f}'_C \end{bmatrix} \qquad (21)$$

A. General Case: ITSC Fault

The new voltage equations after the multiphase Clarke transformation can be written as

$$\begin{bmatrix}\mathbf{v}'_A\\ \mathbf{v}'_B\\ \mathbf{v}'_C\end{bmatrix}=\begin{bmatrix}\mathbf{L}'_{AA} & \mathbf{M}'_{AB} & \mathbf{M}'_{AC}\\ \mathbf{M}'_{BA} & \mathbf{L}'_{BB} & \mathbf{M}'_{BC}\\ \mathbf{M}'_{CA} & \mathbf{M}'_{CB} & \mathbf{L}'_{CC}\end{bmatrix}\frac{\mathrm{d}}{\mathrm{d}t}\begin{bmatrix}\mathbf{i}'_A\\ \mathbf{i}'_B\\ \mathbf{i}'_C\end{bmatrix}+R_{\mathrm{coil}}\begin{bmatrix}\mathbf{i}'_A\\ \mathbf{i}'_B\\ \mathbf{i}'_C\end{bmatrix}+\begin{bmatrix}\boldsymbol{e}'_A\\ \boldsymbol{e}'_B\\ \boldsymbol{e}'_C\end{bmatrix}-\begin{bmatrix}\boldsymbol{C} & \mathbf{0} & \mathbf{0}\\ \mathbf{0} & \boldsymbol{C} & \mathbf{0}\\ \mathbf{0} & \mathbf{0} & \boldsymbol{C}\end{bmatrix}\left(\begin{bmatrix}R_{A1f}\\ 0\\ \vdots\\ 0\end{bmatrix}i_f+\begin{bmatrix}\boldsymbol{M}_{Af}\\ \boldsymbol{M}_{Bf}\\ \boldsymbol{M}_{Cf}\end{bmatrix}\frac{\mathrm{d}i_f}{\mathrm{d}t}\right) \tag{22}$$

where $\mathbf{L}'_{xx}=\boldsymbol{C}\mathbf{L}_{xx}\boldsymbol{C}^{\boldsymbol{T}}$, $\mathbf{M}'_{xy}=\boldsymbol{C}\mathbf{M}_{xy}\boldsymbol{C}^{\boldsymbol{T}}$. "$x$" and "$y$" represent different windings of phases A, B, and C. If inductances calculated by analytical method are employed in this analytical model, then $\mathbf{L}'_{xx}$ and $\mathbf{M}'_{xy}$ become diagonal or block diagonal matrices as follows:

$$\mathbf{L}'_{xx}=\mathrm{diag}\big((L_1+(p-1)M_1),(L_1-M_1),(L_1-M_1),\cdots,(L_1-M_1)\big) \tag{23}$$

and

$$\mathbf{M}'_{AB}=\mathbf{M}'_{BC}=\mathrm{diag}\big((M_2+(p-1)M_1),(M_2-M_1),(M_2-M_1),\cdots,(M_2-M_1)\big) \tag{24}$$

and

$$(\mathbf{M}'_{AC})_{ij}=\begin{cases}M_2+(p-1)M_1 & i=j=1\\ (M_2-M_1)\cos\left(\dfrac{2\pi k}{p}\right) & i=j=2k \text{ or } 2k+1\\ (M_2-M_1)\sin\left(\dfrac{2\pi k}{p}\right) & i=2k, j=2k+1\\ -(M_2-M_1)\sin\left(\dfrac{2\pi k}{p}\right) & i=2k+1, j=2k\\ -(M_2-M_1) & i=j=p\end{cases} \tag{25}$$

In (25), p is assumed to be an even integer, and the integer k can vary from 1 to $(p-2)/2$. Other elements equal to zero in $(\mathbf{M}'_{AC})_{ij}$ are not listed. If p is odd, then the integer k can only vary from 1 to $(p-1)/2$. Therefore, the model is greatly simplified considering that the number of state variables in every first-order differential equation is reduced from $3p+1$ to the minimum value (only 3 to 5 state variables exist after transformation).

The new voltage equation for the short-circuited path can be written by

$$\begin{aligned}&(R_f+R_{A1f})i_f+L_{A1f,A1f}\frac{\mathrm{d}i_f}{\mathrm{d}t}-e_{A1f}-R_{A1f}(\boldsymbol{C}^T\mathbf{i}'_A)_1\\ &=\left(\boldsymbol{C}\boldsymbol{M}_{Af}\right)^T\frac{\mathrm{d}\mathbf{i}'_A}{\mathrm{d}t}+\left(\boldsymbol{C}\boldsymbol{M}_{Bf}\right)^T\frac{\mathrm{d}\mathbf{i}'_B}{\mathrm{d}t}+\left(\boldsymbol{C}\boldsymbol{M}_{Cf}\right)^T\frac{\mathrm{d}\mathbf{i}'_C}{\mathrm{d}t}\end{aligned} \tag{26}$$

where $(\boldsymbol{C}^T\mathbf{i}'_A)_1$ is the first element of the vector $\boldsymbol{C}^T\mathbf{i}'_A$. Finally, the torque equation can be expressed as

$$T_e=\frac{p}{\omega_r}\left(e_Ai_A+e_Bi_B+e_Ci_C-e_{A1f}i_f\right)+T_{cog} \tag{27}$$

It should be mentioned that $\mathbf{v}'_x=[v_x \quad 0 \quad \cdots \quad 0]^T$, $\mathbf{e}'_x=[e_x \quad 0 \quad \cdots \quad 0]^T$. If $i_f=0$, indicating that the machine is healthy, then only three transformed voltage equations with nonzero excited voltages and back-EMFs are useful, others are redundant. This means that, by using the multiphase Clarke transformation, the healthy machine model using branch currents as state variables can be reduced to that using phase currents as state variables. In other words, the mathematical model for machines with parallel-connected coils is the same as that with equivalent series-connected coils under healthy operation if the relationship of equivalent phase (self- and mutual-) inductances between the series and parallel windings are used

$$L_{\mathrm{parallel}}=\frac{1}{p^2}L_{\mathrm{series}} \quad M_{\mathrm{parallel}}=\frac{1}{p^2}M_{\mathrm{series}} \tag{28}$$

Similarly, the relationship of resistance between series and parallel windings can also be established. Finally, the equivalent phase self- and mutual-inductances for parallel-connected coils can be expressed by

$$\begin{cases}(L_{xx})_{\mathrm{parallel}}=\dfrac{1}{p^2}\displaystyle\sum_{i=1}^{p}\sum_{j=1}^{p}(\mathbf{L}_{xx})_{ij}=\dfrac{1}{p}\sum_{j=1}^{p}(\mathbf{L}_{xx})_{1j}\\ \left(M_{xy}\right)_{\mathrm{parallel}}=\dfrac{1}{p^2}\displaystyle\sum_{i=1}^{p}\sum_{j=1}^{p}\left(\mathbf{M}_{xy}\right)_{ij}=\dfrac{1}{p}\sum_{j=1}^{p}\left(\mathbf{M}_{xy}\right)_{1j}\end{cases} \tag{29}$$

B. Special Case: One-Coil Short-Circuit Fault

For the studied machine with parallel-connected coils, the one-coil short-circuit fault is equivalent to one-phase short-circuit fault. When this fault occurs, the circuit branch voltage equations are changed to the following form

$$\begin{bmatrix}\mathbf{v}_A\\ \mathbf{v}_B\\ \mathbf{v}_C\end{bmatrix}=\begin{bmatrix}\mathbf{L}_{AA} & \mathbf{M}_{AB} & \mathbf{M}_{AC}\\ \mathbf{M}_{BA} & \mathbf{L}_{BB} & \mathbf{M}_{BC}\\ \mathbf{M}_{CA} & \mathbf{M}_{CB} & \mathbf{L}_{CC}\end{bmatrix}\frac{\mathrm{d}}{\mathrm{d}t}\begin{bmatrix}\mathbf{i}_{Af}\\ \mathbf{i}_B\\ \mathbf{i}_C\end{bmatrix}+R_{\mathrm{coil}}\begin{bmatrix}\mathbf{i}_{Af}\\ \mathbf{i}_B\\ \mathbf{i}_C\end{bmatrix}+\begin{bmatrix}\mathbf{e}_A\\ \mathbf{e}_B\\ \mathbf{e}_C\end{bmatrix} \tag{30}$$

where $\mathbf{i}_{Af}=[i_{A1}-i_f \quad i_{A2} \quad \cdots \quad i_{Ap}]^T$. The multiphase Clarke transformation in (20) now should be applied to $\mathbf{i}_{Af}$ vector directly, and it can be proven that all coil currents under one-phase short-circuit fault are equal. Here, the current of the first coil A1 is $i_{A1}-i_f$. Under this situation, it is sufficient to use 3-phase currents as state variables to describe the machine behavior, and a system of 5 first-order differential equations is enough to model the machine behavior under the one-coil short-circuit fault (one-phase short-circuit fault). This will make the analysis and simulation much simpler.

V. Simulation Results

Due to the limitation of voltage source excitation in the FE simulations, 3-phase balanced sinusoidal voltages are fed to the studied 3 kW SPM machine to obtain rated torque before fault and its rotor mechanical speed is kept constant during the whole operation period.

A. Half-a-Coil (50% Turns of a Coil) Short-Circuited

Different fault severities such as single-turn, half-a-coil and one-coil short-circuits have been investigated, however, due to page limit, only some representative results of the half-a-coil short-circuit fault have been provided in this section. For the half-a-coil short-circuited case, $h_a=h_s/n_c$ and $h_b=(0.5n_c+1)h_s/n_c$ are chosen. Fig. 6 shows the currents in the faulty coil A1 before and after the half-a-coil short-circuit fault. It could be easily seen that there is a very small discrepancy in simulation results from the two models. Although the short-circuit current is much higher than the rated current (about 28 times), relatively low number of turns being short-circuited

means that the impact of fault on on-load torque is less significant, as shown in Fig. 7.

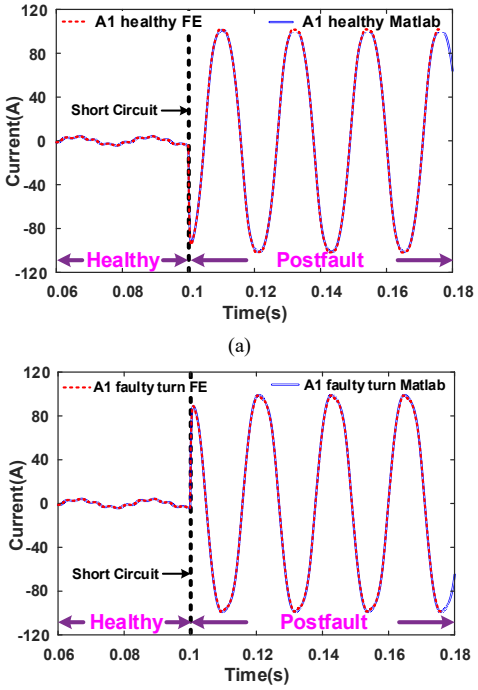

Fig. 6 Current waveforms before and after half-a-coil short-circuit fault. (a) In remaining healthy turns and (b) in short-circuited turns.

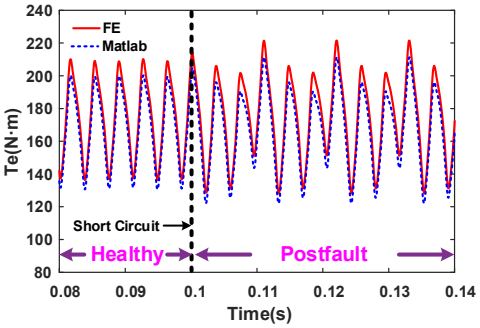

Fig. 7 On-load torque of the 3 kW SPM machine before and after the half-a-coil short-circuit fault.

On the other hand, some branch currents of phases B and C are shown in Fig. 8. It is found that not all branch currents in the remaining healthy phase windings are the same. In fact, the branch currents of phases B and C next to the faulty branch of phase A are significantly affected, meaning that the changes in i_{B1}, i_{B16}, i_{C1}, and i_{C16} are greater compared with other branch currents in phases B and C when the ITSC fault occurs in A1 branch. Although it is not shown here, the branch currents i_{B2} to i_{B15} in phase B (or i_{C2} to i_{C15} in phase C) are almost the same. In addition, it is found that the behavior of branch currents of phase C is different from that of phase B. This is mainly because the mutual inductances $M_{A1B1} \neq M_{A1C1}$ and $M_{A1B16} \neq M_{A1C16}$. If both of them were equal, then the two branch inductance matrices $\mathbf{M}_{AB} = \mathbf{M}_{AC}$ and $\mathbf{M}_{Bf} = \mathbf{M}_{Cf}$, leading to the same behaviour of branch currents in the two phases after the ITSC fault.

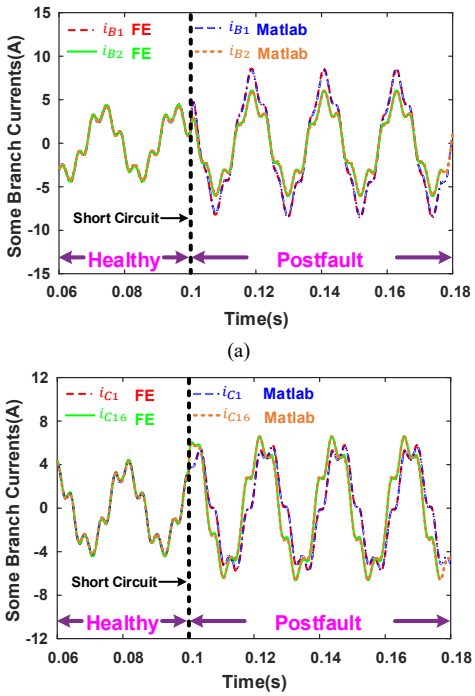

Fig. 8 Some branch currents of phases B and C. (a) phase B and (b) phase C.

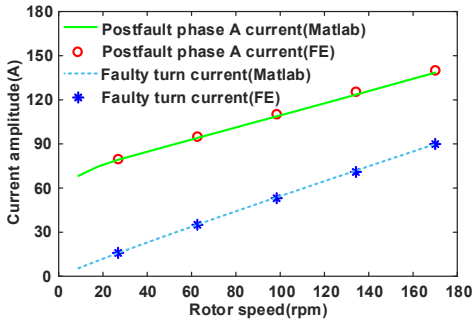

Fig. 9 Peak currents of phase A and faulty turns before and after half-a-coil short-circuit fault.

B. *Different Speeds*

It is worth mentioning that the results in the previous section are obtained under the rated speed only. To further verify the accuracy of the proposed analytical model, simulations under half-a-coil short-circuit fault at different rotor speeds have been carried out. The amplitudes of currents of phase A and faulty turns are shown in Fig. 9. It is found that the ITSC current and postfault phase current increase almost linearly with the rotor speed. This is mainly due to the increase in back-EMF of the short-circuited turns. If the rotor speed keeps increasing, the fault current can be much higher than the rated current. This means that early fault detection is critical, otherwise, if the fault is left undetected and untreated, the affected coils could be overheated, leading to catastrophic damage to the entire machine.

VI. Experimental Validation

A. *Prototype and Test Rig*

A small-scale 12-slot 4-pole SPM machine prototype has been built to validate the proposed fault model. The key data

Table III Specifications of 12-slot 4-pole SPM machine

Rated speed (rpm)	400	Stator outer diameter (mm)	100
Rated current rms (A)	2.5	Rotor outer diameter (mm)	49
Series turns/coil	40	Air gap length (mm)	1
Slots/poles	12/4	Stack length (mm)	50

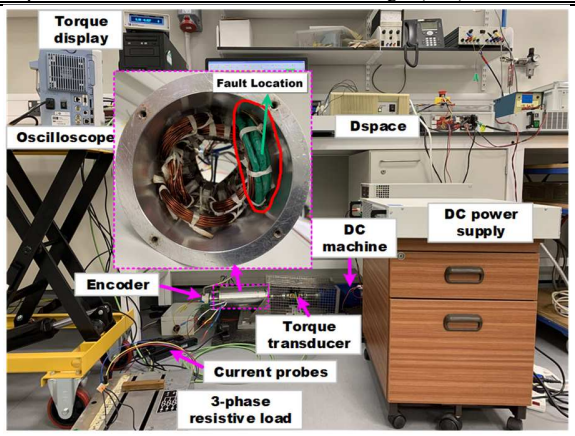

Fig. 10 Test rig.

of this prototype machine are listed in Table III. The stator and test rig of the prototype machine are both shown in Fig. 10.

It is worth mentioning that single layer windings are used for this 12-slot 4-pole SPM prototype machine, thus it will only have two parallel branches in each phase. All the coils of the prototype machine can be connected outside of the machine housing so that the branch currents in all phases can be measured. Using this prototype machine, three fault scenarios can be carried out: one-coil, half-a-coil, and single-turn short-circuit faults. In addition, all the faults are introduced in A1 coil. As the main purpose of the experiments is to validate the proposed fault model, the SPM machine will be used as a generator driven by a dc machine, and its 3-phase terminals are connected to an adjustable 3-phase resistive load bank, which replaces the 3-phase voltage sources in Fig. 1. In this way, no inverter is required to drive the SPM machine, avoiding the necessity of complicated control schemes.

B. Inductances

The analytical method for inductance calculation developed in section III has also been applied to this 12-slot 4-pole SPM machine. Some representative results have been provided in Table IV, where all the FE inductances in Table IV are average values over one electrical period.

A generally good agreement can be observed between the analytical and 2D linear FE results. However, it is found that the length of the end windings at each side of this prototype machine is almost equal to the stack length. This means that the influence of the end windings on inductance values cannot be neglected. Meanwhile, the core saturation also has a significant impact on the inductance values, makes the inductances much smaller.

In order to obtain more accurate inductance results, a 3D FE model has been built using JMAG. The obtained 3D FE nonlinear inductances are compared with the measured ones by using the Hioki IM3570 Impedance Analyzer, as shown in Table V. It can be observed from Table V that most of the relative errors between the 3D FE nonlinear and measured inductances are generally within an acceptable range. However,

Table IV Inductances related to A1 coil in mH

Method	L_{A1A1}	M_{A1A2}	M_{A1B1}	M_{A1B2}
Analytical	0.82	-0.246	0.082	-0.246
2D FE (Linear)	0.78	-0.224	0.074	-0.224
Difference (%)	5.1	9.8	10.8	9.8
2D FE (Nonlinear)	0.508	-0.08	0.0075	-0.112
Difference (%)	53.5	180	886.7	100

Note: the difference (%) in the last row is between the 2D FE (linear) and 2D FE (nonlinear).

Table V 3D FE and measured inductances in mH of the prototype machine

Method	L_{A1A1}	L_{A2A2}	M_{A1B1}	M_{A1B2}
3D FE (Nonlinear)	0.821	0.688	0.0063	-0.132
Measured	0.857	0.812	0.0192	-0.172
Difference (%)	-4.2	-15.3	-67.2	-23.2

the relative error of M_{A1B1} exceeds 50%. This is mainly because the absolute value of M_{A1B1} is very small, so the measured value may not be reliable due to potential measurement errors.

In addition, due to its very small value, its impact on machine performance prediction can be negligible, as will be investigated in the following section. As for the 3D FE nonlinear inductances related to the short-circuited turns, they can be calculated by using the inductances related to coil A1.

C. Branch and Faulty Currents under Half-a-Coil Short-Circuit Fault

All the three fault scenarios (single-turn, half-a-coil, and one-coil short-circuit faults) have been carried out under different speeds and loads to validate the proposed fault model, and the measured and simulated results generally match well. However, due to page limit, only some results of half-a-coil short-circuit fault are shown.

In addition, it is worth mentioning that for this machine, the cogging torque is quite large and its amplitude is comparable to the rated torque. As a result, the cogging torque causes large speed ripples and could prevent the machine from spinning at low speed. One example is that when the machine is rotating at 900rpm, the maximum speed ripple is about 200rpm (22%). This is why the position encoder (see Fig. 10) is required to capture the speed ripples accurately so that the predicted current profiles will be closer to the measured ones.

A 3-phase resistive load of $R_{load} = 1.2\Omega$ is connected to the 3-phase terminals of this prototype machine to limit the amplitude of the branch and phase currents when the half-a-coil short-circuit fault is introduced. The speed and current data are collected when the average speed of the prototype machine is about 900rpm. This relatively high speed is chosen in order to reduce the impact of speed ripple on the current predictions. At the same time, the branch currents and phase currents are shown in Fig. 11 and Fig. 12, respectively.

It should be mentioned that the predicted branch and phase currents by using 3D FE and measured inductances in the fault model are almost the same. Therefore, only the predicted results using measured inductances have been provided in Fig. 11 and Fig. 12. It can be seen from Fig. 11 that the measured and predicted branch currents match well, this is the same for

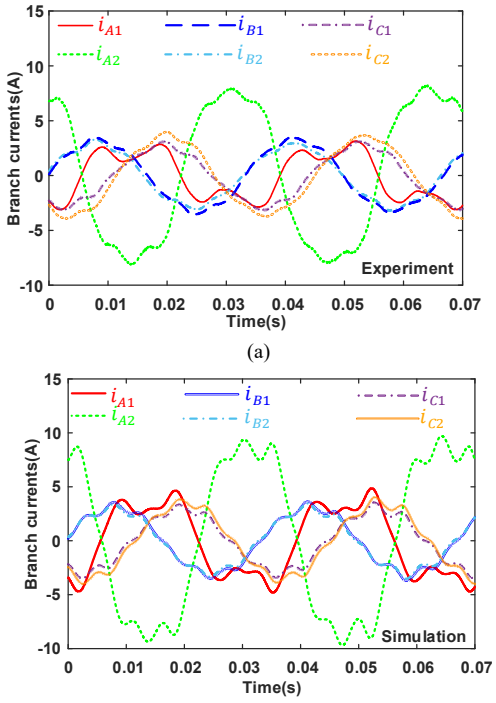

Fig. 11 Branch currents under the half-a-coil short-circuit fault. (a) Measured and (b) predicted.

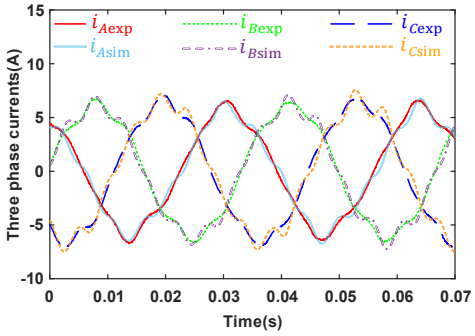

Fig. 12 Measured and predicted 3-phase currents under half-a-coil short-circuit fault.

the measured and predicted three phase currents as shown in Fig. 12.

The predicted fault current i_{A1f} in the short-circuited turns (using both 3D FE and measured inductances) has also been compared against the measured i_{A1f}, as shown in Fig. 13. Again, the predicted i_{A1f} using 3D FE and measured inductances match very well, although both are slightly larger than the measured i_{A1f}, which may be due to measurement errors.

D. Different Loads and Speeds

For completeness of the model verification, further tests with different loads and speeds under the one-coil short-circuited fault have also been carried out, the results of which are shown in Fig. 14. It can be seen that the currents (peak value) in the short-circuited coil A1 and faulty phase A with two different resistive loads and different rotor speeds from measurement and simulation match well. Therefore, it can be concluded that

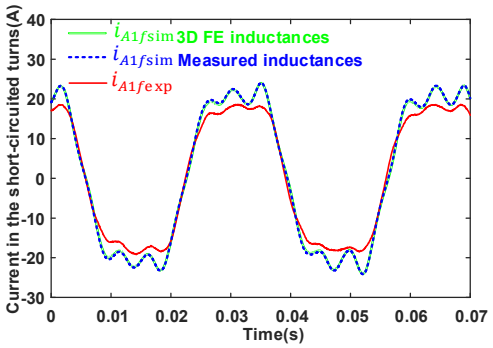

Fig. 13 Predicted and measured fault currents (i_{A1f}) in the short-circuited turns.

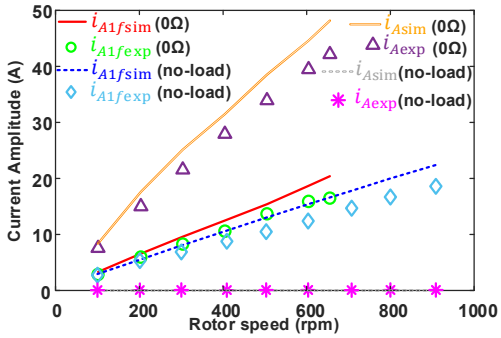

Fig. 14 Amplitudes of current of short-circuited coil and faulty phase under different resistive loads and speeds.

the proposed fault model is accurate in predicting the ITSC fault behaviors of SPM machines.

VII. Conclusion

This paper presents a general analytical model in a compact matrix form for PM wind generators with parallel-connected coils under ITSC fault. To simplify the fault model with analytical inductances, the multiphase Clarke transformation has been proposed. Such model simplification method may be extended to other types of electrical machines with similar winding configurations, no matter how many phases the machines have.

For the sake of generality, different fault scenarios have been investigated using the proposed analytical model, in which the branch currents are used as state variables. First of all, the inductances in the faulty machine model have been calculated by the proposed analytical approach, which have been compared against FE predictions when core saturation is neglected. Overall good agreement has been observed except for the mutual inductances between coils farther apart. However, these mutual inductances are very small. Then, these inductances have been used in the faulty machine model built in Matlab/Simulink for a 3 kW machine to predict machine performance such as healthy and short-circuit currents and on-load torque before and after various short-circuit faults. The accuracy of the proposed analytical fault model has been validated by 2D time-stepping FE simulations. The analytical model developed in this paper can be very useful for model-based fault detection and mitigation of large wind power generators, for which the FE or magnetic equivalent circuit modelling can be very time-consuming due to large number of slots and poles. Finally, a small scale 12-slot 4-pole SPM

machine prototype with the same winding configuration as that of large wind power generators has been built to further validate the accuracy of the proposed fault model. It is worth mentioning that, in general, the saturation level of MW machines would be higher than small-scale machines. If heavy saturation needs to be considered, rather than using the analytically obtained inductances, the ones obtained by direct FEA (non-linear) can be used in the developed fault model to predict the machine behavior under ITSC fault.

APPENDIX A

Branch inductance matrices are described as

$$\mathbf{L}_{xx} = \begin{bmatrix} L_{x1x1} & M_{x1x2} & M_{x1x3} & \cdots & M_{x1xp} \\ M_{x2x1} & L_{x2x2} & M_{x2x3} & \cdots & M_{x2xp} \\ M_{x3x1} & M_{x3x2} & L_{x3x3} & \cdots & M_{x3xp} \\ \vdots & \vdots & \vdots & \ddots & \vdots \\ M_{xpx1} & M_{xpx2} & M_{xpx3} & \cdots & L_{xpxp} \end{bmatrix} \tag{31}$$

$$\mathbf{M}_{xy} = \left(\mathbf{M}_{yx}\right)^T = \begin{bmatrix} M_{x1y1} & M_{x1y2} & M_{x1y3} & \cdots & M_{x1yp} \\ M_{x2y1} & M_{x2y2} & M_{x2y3} & \cdots & M_{x2yp} \\ M_{x3y1} & M_{x3y2} & M_{x3y3} & \cdots & M_{x3yp} \\ \vdots & \vdots & \vdots & \ddots & \vdots \\ M_{xpy1} & M_{xpy2} & M_{xpy3} & \cdots & M_{xpyp} \end{bmatrix} \tag{32}$$

where x and y designate the phase windings, namely, A, B and C. $\mathbf{L}_{xx}$ describes all the inductive couplings of the same or different coils/branches in the same phase winding, and $\mathbf{M}_{xy}$ describes the inductive couplings between different coils/branches in two different phase windings. In addition, both of them have the size of $p \times p$, and p is the number of pole pairs.

For example, in (31), L_{AiAi} ($i = 1,2,\cdots,p$) is the self-inductance of branch Ai winding, and M_{AiAj} ($i \neq j; i = 1,2,\cdots,p; j = 1,2,\cdots,p$) is the mutual inductance between two different branches Ai and Aj in phase A winding. Similar explanation applies to other branch inductance matrices. It is worth noting that all these branch inductance matrices are circulant matrices. One important characteristic of circulant matrices is that the elements of each row are identical to those of the previous row, but are moved one position to the right and wrapped around [17], [18]. Its mathematical form is as follows

$$\mathrm{circ}(c_0, c_1, \cdots, c_{p-1}) = \begin{bmatrix} c_0 & c_1 & c_2 & \cdots & c_{p-1} \\ c_{p-1} & c_0 & c_1 & \cdots & c_{p-2} \\ c_{p-2} & c_{p-1} & c_0 & \cdots & c_{p-3} \\ \vdots & \vdots & \vdots & \ddots & \vdots \\ c_1 & c_2 & c_3 & \cdots & c_0 \end{bmatrix} \tag{33}$$

As for faulty inductance vectors, they can be written as

$$\begin{cases} \boldsymbol{M}_{Af} = [L_{A1f,A1f} + M_{A1h,A1f} \quad M_{A2,A1f} \quad \cdots \quad M_{Ap,A1f}]^T \\ \boldsymbol{M}_{Bf} = [M_{B1,A1f} \quad M_{B2,A1f} \quad \cdots \quad M_{Bp,A1f}]^T \\ \boldsymbol{M}_{Cf} = [M_{C1,A1f} \quad M_{C2,A1f} \quad \cdots \quad M_{Cp,A1f}]^T \end{cases} \tag{34}$$

It can be seen that $L_{A1f,A1f}$ is the self-inductance of the short-circuited turns and $M_{A1h,A1f}$ represents the mutual inductance between the remaining healthy turns and short-circuited turns of the faulty coil, A1.

APPENDIX B

The multiphase Clarke transformation matrix is shown in (35) [19], [20].

$$\boldsymbol{C} = \sqrt{\frac{2}{p}} \begin{bmatrix} \frac{1}{\sqrt{2}} & \frac{1}{\sqrt{2}} & \frac{1}{\sqrt{2}} & \cdots & \frac{1}{\sqrt{2}} & \cdots & \frac{1}{\sqrt{2}} \\ 1 & \cos\left(-\frac{2\pi}{p}\right) & \cos\left(-2\times\frac{2\pi}{p}\right) & \cdots & \cos\left(-m\times\frac{2\pi}{p}\right) & \cdots & \cos\left(-(p-1)\times\frac{2\pi}{p}\right) \\ 0 & \sin\left(-\frac{2\pi}{p}\right) & \sin\left(-2\times\frac{2\pi}{p}\right) & \cdots & \sin\left(-m\times\frac{2\pi}{p}\right) & \cdots & \sin\left(-(p-1)\times\frac{2\pi}{p}\right) \\ \vdots & \vdots & \vdots & \vdots & \vdots & \vdots & \vdots \\ 1 & \cos\left(-k\times\frac{2\pi}{p}\right) & \cos\left(-2\times k\times\frac{2\pi}{p}\right) & \cdots & \cos\left(-m\times k\times\frac{2\pi}{p}\right) & \cdots & \cos\left(-(p-1)\times k\times\frac{2\pi}{p}\right) \\ 0 & \sin\left(-k\times\frac{2\pi}{p}\right) & \sin\left(-2\times k\times\frac{2\pi}{p}\right) & \cdots & \sin\left(-m\times k\times\frac{2\pi}{p}\right) & \cdots & \sin\left(-(p-1)\times k\times\frac{2\pi}{p}\right) \\ \vdots & \vdots & \vdots & \vdots & \vdots & \vdots & \vdots \\ 1 & \cos\left(-\left(\frac{p-2}{2}\right)\times\frac{2\pi}{p}\right) & \cos\left(-2\times\left(\frac{p-2}{2}\right)\times\frac{2\pi}{p}\right) & \cdots & \cos\left(-m\times\left(\frac{p-2}{2}\right)\times\frac{2\pi}{p}\right) & \cdots & \cos\left(-(p-1)\times\left(\frac{p-2}{2}\right)\times\frac{2\pi}{p}\right) \\ 0 & \sin\left(-\left(\frac{p-2}{2}\right)\times\frac{2\pi}{p}\right) & \sin\left(-2\times\left(\frac{p-2}{2}\right)\times\frac{2\pi}{p}\right) & \cdots & \sin\left(-m\times\left(\frac{p-2}{2}\right)\times\frac{2\pi}{p}\right) & \cdots & \sin\left(-(p-1)\times\left(\frac{p-2}{2}\right)\times\frac{2\pi}{p}\right) \\ \frac{1}{\sqrt{2}} & -\frac{1}{\sqrt{2}} & \frac{1}{\sqrt{2}} & \cdots & (-1)^m\frac{1}{\sqrt{2}} & \cdots & -\frac{1}{\sqrt{2}} \end{bmatrix} \tag{35}$$

In (35), one assumption is made that the number of pole pairs is even. If the number of pole pairs is odd, then the last row in (35) should be deleted and all $\left(\frac{p-2}{2}\right)$ terms appeared in the last three rows should be replaced by $\left(\frac{p-1}{2}\right)$.

REFERENCES

[1] B. Lu, Y. Li, X. Wu, and Z. Yang, "A review of recent advances in wind turbine condition monitoring and fault diagnosis," in *2009 IEEE Power Electronics and Machines in Wind Applications*, Jun. 2009, pp. 1–7.

[2] N. M. A. Freire and J. Marques Cardoso Antonio, "Fault detection and condition monitoring of PMSGs in offshore wind turbines," *Machines*, vol. 9, no. 11, p. 260, 2021.

[3] S. Nandi, H. A. Toliyat, and X. Li, "Condition monitoring and fault diagnosis of electrical motors--a review," *IEEE Trans. Energy Convers.*, vol. 20, no. 4, pp. 719–729, 2005.

[4] A. H. Bonnett and G. C. Soukup, "Cause and analysis of stator and rotor failures in three-phase squirrel-cage induction motors," *IEEE Trans. Ind. Appl.*, vol. 28, no. 4, pp. 921–937, Jul. 1992.

[5] Z. T. Mei, G. J. Li, Z. Q. Zhu, R. Clark, A. Thomas, and Z. Azar, "Scaling effect on inter-turn short-circuit of PM machines for wind power application," in *2021 IEEE International Electric Machines and Drives Conference (IEMDC)*, 2021, pp. 1–8.

[6] S. E. Dallas, A. N. Safacas, and J. C. Kappatou, "Interturn stator faults analysis of a 200-MVA hydrogenerator during transient operation using FEM," *IEEE Trans. Energy Convers.*, vol. 26, no. 4, pp. 1151–1160, Dec. 2011.

[7] B. Ge, S. Xiao, Z. Liu, D. Tao, and X. Sun, "Improved model of synchronous generators internal faults based on circuit-coupled FEM," *IEEE Trans. Energy Convers.*, vol. 32, no. 3, pp. 876–884, Sep. 2017.

[8] G. Forstner, A. Kugi, and W. Kemmetmüller, "A magnetic equivalent circuit based modeling framework for electric motors applied to a PMSM with winding short circuit," *IEEE Trans. Power Electron.*, vol. 35, no. 11, pp. 12285–12295, 2020.

[9] X. H. Wang, Y. G. Sun, B. Ouyang, W. J. Wang, Z. Q. Zhu, and D. Howe, "Transient behaviour of salient-pole synchronous machines with internal stator winding faults," *Proc. Inst. Electr. Eng.—Electr. Power Appl.*, vol. 149, no. 2, pp. 143–151, Mar. 2002.

[10] X. Tu, L. Dessaint, M. E. Kahel, and A. O. Barry, "A new model of synchronous machine internal faults based on winding distribution," *IEEE Trans. Ind. Electron.*, vol. 53, no. 6, pp. 1818–1828, Dec. 2006.

[11] X. Tu, L. Dessaint, N. Fallati, and B. D. Kelper, "Modeling and real-time simulation of internal faults in synchronous generators with parallel-connected windings," *IEEE Trans. Ind. Electron.*, vol. 54, no. 3, pp. 1400–1409, Jun. 2007.

[12] M. B. K. Bouzid, G. Champenois, A. Maalaoui, and S. Tnani, "Efficient simplified physical faulty model of a permanent magnet synchronous generator dedicated to the stator fault diagnosis part I: faulty model conception," *IEEE Trans. Ind. Appl.*, vol. 53, no. 3, pp. 2752–2761, May 2017.

[13] B. Gu, J. Choi, and I. Jung, "Development and analysis of interturn short fault model of PMSMs with series and parallel winding connections," *IEEE Trans. Power Electron.*, vol. 29, no. 4, pp. 2016–2026, Apr. 2014.

[14] H. Qian, H. Guo, and X. Ding, "Modeling and analysis of interturn short fault in permanent magnet synchronous motors with multistrands windings," *IEEE Trans. Power Electron.*, vol. 31, no. 3, pp. 2496–2509, Mar. 2016.

[15] J. R. Hendershot and T. J. E. Miller, *Design of Brushless Permanent-Magnet Machines*. Motor Design Books, 2010.

[16] T. A. Lipo, *Analysis of Synchronous Machines*, 2nd ed. CRC Press, 2012.

[17] P. J. Davis, *Circulant Matrices*. Wiley, 1979.

[18] D. C. White and H. H. Woodson, *Electromechanical Energy Conversion*. Wiley, 1959.

[19] J. Huang, M. Kang, J. Yang, H. Jiang, and D. Liu, "Multiphase machine theory and its applications," in *2008 International Conference on Electrical Machines and Systems*, 2008, pp. 1–7.

[20] A. G. Yepes, J. A. Riveros, J. Doval-Gandoy, F. Barrero, Ó. Lopez, B. Bogado, M. Jones and E. Levi, "Parameter identification of multiphase induction machines with distributed windings—Part 1: sinusoidal excitation methods," *IEEE Trans. Energy Convers.*, vol. 27, no. 4, Art. no. 4, 2012.